interactions between the PRP9, PRP11, and SPP91 proteins we have characterized here suggest the existence of a highly conserved multimolecular complex that is required for prespliceosome assembly. The third component of the SF3a factor, the 120-kD polypeptide, is a likely candidate for the SPP91 mammalian homolog. Thus the PRP9-PRP11-SPP91 complex may serve as a bridge between the U1 and U2 snRNPs to form the prespliceosome and to commit pre-mRNAs to the splicing pathway (*25*). The binding sites of this complex to the pre-mRNA or to the U1 and U2 snRNPs, or both, remain to be identified.

REFERENCES AND NOTES

1. M. R. Green, *Annu. Rev. Cell Biol.* **7**, 559 (1991).
2. M. J. Moore, C. C. Query, P. A. Sharp, in *The RNA World*, R. Gesteland and J. Atkins, Eds. (Cold Spring Harbor Press, Cold Spring Harbor, NY, 1993), vol. 24.
3. B. C. Rymond and M. Rosbash, in *The Molecular and Cellular Biology of the Yeast* Saccharomyces (Cold Spring Harbor Laboratory Press, Cold Spring Harbor, NY, 1992), pp. 143–192.
4. T. H. Chang, M. W. Clark, A. J. Lustig, M. E. Cusick, J. Abelson, *Mol. Cell. Biol.* **8**, 2379 (1988).
5. P. Legrain and A. Choulika, *EMBO J.* **9**, 2775 (1990).
6. N. Abovich, P. Legrain, M. Rosbash, *Mol. Cell. Biol.* **10**, 6417 (1990).
7. C. Chapon and P. Legrain, *EMBO J.* **11**, 3279 (1992).
8. J. Arenas and J. Abelson, *Proc. Natl. Acad. Sci. U.S.A.* **90**, 6771 (1993).
9. P. Legrain, C. Chapon, F. Galisson, *Genes Dev.* **7**, 1390 (1993).
10. P. Legrain and C. Chapon, unpublished results.
11. I. Herskowitz, *Nature* **329**, 219 (1987).
12. S. Ruby and J. Abelson, personal communication.
13. C. T. Chien, P. L. Bartel, R. Sternglanz, S. Fields, *Proc. Natl. Acad. Sci. U.S.A.* **88**, 9578 (1991).
14. S. Fields and O. K. Song, *Nature* **340**, 245 (1989).
15. K. Schappert and J. D. Friesen, *Mol. Gen. Genet.* **226**, 277 (1991).
16. The *prp9-C423* mutation is a substitution of the Cys^{423} residue located in the PRP9 CH2 motif (*5*). This mutation affects the homodimerization of the PRP9 protein but does not interfere with the binding to SPP91 (*9*).
17. P. T. Sillekens, R. P. Beijer, W. J. Habets, W. van Venrooij, *Nucleic Acids Res.* **16**, 8307 (1988).
18. R. L. Nelissen *et al.*, *ibid.* **19**, 449 (1991).
19. S. E. Behrens, K. Tyc, B. Kastner, J. Reichelt, R. Lührmann, *Mol. Cell. Biol.* **13**, 307 (1993).
20. S. Behrens, F. Galisson, P. Legrain, R. Lührmann, *Proc. Natl. Acad. Sci. U.S.A.*, in press.
21. A. Krämer and U. Utans, *EMBO J.* **10**, 1503 (1991).
22. R. Brosi, K. Gröning, S. Behrens, R. Lührmann, A. Krämer, *Science* **262**, 102 (1993).
23. R. Brosi, H. P. Hauri, A. Krämer, *J. Biol. Chem.*, in press.
24. M. Bennett and R. Reed, *Science* **262**, 105 (1993).
25. P. Legrain and M. Rosbash, *Cell* **57**, 573 (1989).
26. J. Ma and M. Ptashne, *ibid.* **51**, 113 (1987).
27. L. Guarente, R. R. Yocum, P. Gifford, *Proc. Natl. Acad. Sci. U.S.A.* **79**, 7410 (1982).
28. We inserted polymerase chain reaction (PCR)–derived DNA fragments encoding the appropriate PRP9, PRP11, or SPP91 open reading frames at the Bam HI site of the pGAD2F and pMA424 plasmids (*9, 13, 26*).

29. We are indebted to S. Fields and M. Werner for plasmids and strains used for the two-hybrid system. We thank J. Arenas, J. Abelson, R. Brosi, A. Krämer, M. Bennett, R. Reed, and S. Ruby for communicating unpublished results. We also thank G. Chanfreau, A. Jacquier, A. Krämer, A. Korman, and C. Transy for numerous discussions and for critically reading the manuscript. Finally, we acknowledge the continuous support and interest of B. Dujon in this work. This work was partly supported by the Universite Pierre et Marie Curie and the CNRS (URA 1149).

12 July 1993; accepted 9 August 1993

Ordered Restriction Maps of *Saccharomyces cerevisiae* Chromosomes Constructed by Optical Mapping

David C. Schwartz,* Xiaojun Li,† Luis I. Hernandez,† Satyadarshan P. Ramnarain, Edward J. Huff,† Yu-Ker Wang†

A light microscope–based technique for rapidly constructing ordered physical maps of chromosomes has been developed. Restriction enzyme digestion of elongated individual DNA molecules (about 0.2 to 1.0 megabases in size) was imaged by fluorescence microscopy after fixation in agarose gel. The size of the resulting individual restriction fragments was determined by relative fluorescence intensity and apparent molecular contour length. Ordered restriction maps were then created from genomic DNA without reliance on cloned or amplified sequences for hybridization or analytical gel electrophoresis. Initial application of optical mapping is described for *Saccharomyces cerevisiae* chromosomes.

Construction of physical maps for eukaryotic chromosomes is laborious and difficult, in part because many of the current procedures for mapping and sequencing DNA were originally designed to analyze genes rather than genomes (*1*). The electrophoretic methods that are widely used in mapping offer the advantage of good size resolution, even for large molecules, but require preparation of DNA in bulk amounts from sources such as genomic DNA or yeast artificial chromosomes (YACs) (*2*). In contrast, single-molecule techniques, such as fluorescence in situ hybridization (FISH), make use of only a limited number of chromosomes (*3*), but have not yet attained a sizing resolution comparable to that of pulsed electrophoresis (*4*). Ideally, one would like to be able to combine the sizing power of electrophoresis with the intrinsic ordering capability of FISH in order to construct accurate restriction maps very rapidly. The methodology described in this report, which we refer to as optical mapping, approaches this ideal by imaging stained, single, deproteinized DNA molecules during restriction enzyme digestion. This allows direct, ordered mapping of restriction sites.

In brief, a fluid flow was used to stretch out DNA molecules dissolved in molten agarose and fix them in place during gelation (*4*). The gelation process restrains elongated molecules from relaxing to a random coil conformation during enzymatic cleavage. A restriction enzyme is added to the molten agarose–DNA mixture, and cutting is triggered by the diffusion of Mg^{2+} into the gelled mixture, which has been mounted on a microscope slide. Fluorescence microscopy coupled with digital image processing techniques were used to record, at regular intervals, cleavage sites, which are visualized by the appearance of growing gaps in imaged molecules (*5*) and bright, condensed pools or "balls" of DNA on the fragment ends flanking the cut site. These balls form shortly after cleavage as a result of coil relaxation at the new ends. The size of the resulting fragments was determined in two ways: by measurement of the relative fluorescence intensities of the products and by measurement of the relative apparent DNA molecular lengths in the fixating gel. Maps are subsequently assembled by recording the order of the sized fragments (*6*). Averaging a small number of molecules rather than using only one improves accuracy and permits rejection of unwanted molecules (*7*).

Large DNA molecules can be stretched out in molten agarose by flow forces and then rapidly fixed in place by agarose gelation, without application of electrical fields (*4*). Experimentally, the kinetics of gelation are controlled by temperature and optimization of the annealing conditions. For our analysis, DNA coils must be critically stretched: too much and the molecule becomes difficult to image, too little and there is insufficient tension to reveal cut sites. Excessively stretched molecules present too little fluorochrome per imaging pixel, so that measured molecular intensities approach background values. Additionally,

W. M. Keck Laboratory for Biomolecular Imaging, Department of Chemistry, New York University, New York, NY 10003.

*To whom correspondence should be addressed.
†These authors contributed equally to this work.

the fixation process has to be gentle enough to permit some coil slippage to reveal cut sites, since completely immobilized molecules cannot reveal relaxation events. Taking these and other considerations into account, we have practically optimized our fixation conditions to produce molecules spanning approximately 20 to 30% of their curvilinear contour lengths.

How DNA molecules are entrapped by agarose gelation is not known. Imaged, stretched molecules show bright, round pools of coil at their ends, evidence of chain relaxation. The pool sizes range from 1 to 3 μm. Segmental pools are also observed to form internally, and then disappear, as local pockets of coil tension equilibrate with each other. As a DNA molecule relaxes within the train of contiguous gel pores it spans, the segmental density increases, and segments can even be seen to spill over into neighboring pore spaces. The detailed relaxation mechanism is a complex one (*8*). Gaps appear because a molecule experiences an effective tension, since the configurational entropy of the elongated polymer is lower than that of the relaxed state.

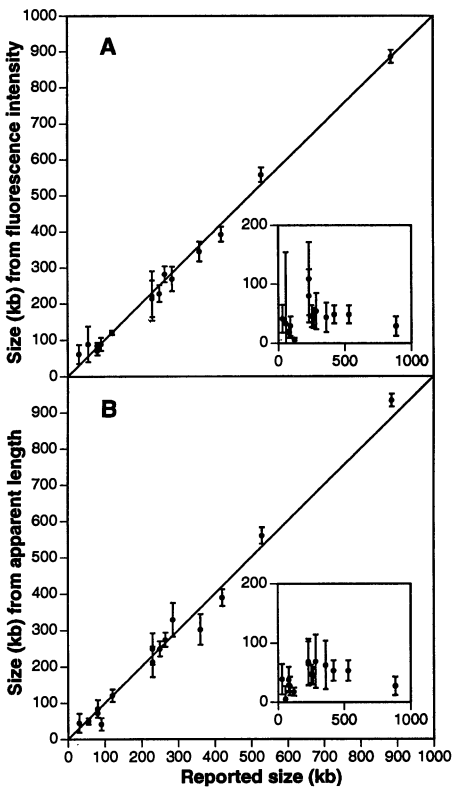

Fig. 1. Optical mapping sizing results for Not I endonuclease restriction fragments from *S. cerevisiae* chromosomes 1, 5, 8, 11, 13, and 16 calculated as described (*6, 7*) and plotted against published results (*10*). The diagonal line is for reference. Typical fragment images are shown in Fig. 2. Typically, 10 to 35 fragments were imaged out of which roughly half were discarded because of poor focus, insufficient initial lengths, or cut scoring ambiguities. (**Inset**) Estimate of population SD (in kilobases). Error bars represent 90% confidence (*7*) on means (main graph) or SD (inset). (**A**) Relative intensity determination of fragment sizes. (**B**) Relative apparent length determination of fragment sizes.

The first step in map construction is to determine the number of cleavage sites within a molecule by examining histograms of cuts per molecule and corresponding cleavage patterns. Because the rates of enzymatic cleavage by different restriction enzymes are variable, careful adjustment of the timing is critical. We wanted cleavage to occur only after molecular fixation was complete because premature reactions would disrupt attempts to order fragments. We solved this timing problem by premixing the agarose-DNA solution with restriction enzyme, at 37°C, and triggering the reaction by diffusing Mg^{2+} into the viewing field, without disturbing the gel (*4*). All possible cleavage sites did not appear simultaneously; instead, cuts usually appeared within 5 min of each other. A typical mounted sample contained approximately 3 to 5 molecules within a single viewing field, and overall roughly 50 to 95% of them showed evidence of one or more cuts (*9*).

The next step was to determine the size of the resulting restriction fragments. For this purpose we have developed two complementary approaches, one based on relative fragment fluorescence intensity and the second on apparent relative length measurements.

Microscope-based intensity measurements are difficult to perform because of their dependence on many variables, including camera control and illumination intensity. By calculating the relative intensity of two fragments (from the same parental molecule), we allow one of the fragments to serve as an internal intensity reference for the other. Relative intensities are converted to kilobases by multiplying by the known or independently determined chromosome size (6). Figure 1A shows the sizes determined for a series of yeast chromosome Not I restriction fragments measured optically and plotted against published values derived from electrophoresis-based measurements (*10*). Points close to the diagonal line are in good agreement. Excluding the two short fragments less than 60 kb and the low-resolution 8-bit chromosome 5 and 8 data, the pooled SD was 36 kb (Fig. 1A, inset). The average of the coefficients of variation was 16%, which is comparable to routine pulsed electrophoresis size determinations. The correlation with published results is excellent: The average of the relative errors is 5%, whereas the published errors average 4% (*7, 10*). Due in part to the intensity normalization procedure, the precision becomes lower for very small fragments, and size agreement is poor for the measurements of the 30- and 55-kb DNAs. Fluorescence intensity measurements report a size of these fragments almost twice that of the above values.

One test of the validity of relative fluorescence intensity measurements is to monitor the constancy of fragment intensities over a usable range of molecular relaxation conditions. This requirement is most critically tested when restriction fragments differ greatly in size. Our results show that intensities remain relatively constant over a wide size range despite a three- to fourfold change in measured molecular length (*11*). We attribute this beneficial effect in part to the mild fixation conditions, so that Brownian motion can vibrate the elongated coil along the z axis; this motion is clearly observed on the live video monitor as digestion proceeds. By averaging frames over a 1-s interval, we observe most of the DNA as it moves through the focal plane and within the gel pores.

For measurement of the relative apparent length, each gel-embedded restriction fragment is assumed to have equal coil density, on the average. Again, we converted relative apparent lengths to kilobases by multiplying by the chromosome size (6). Then, we averaged the apparent lengths of restriction fragments, obtaining accurate sizes from as few as four molecules (*7*). Relative determinations of apparent length were standardized against the same set of restriction fragments as in the fluorescence intensity measurements, and these results (Fig. 1B) show a similar average relative error of 16% (excluding the 30- and 90-kb fragments). The pooled SD was 47 kb (Fig. 1B, inset); the average of the coefficients of variation was 29%.

Length measurements can be used to evaluate fragments that are out of focus, whereas blurry, out-of-focus images confound intensity-based measurements. Additionally, size determinations of small fragments are better by length than by intensity. The size of the 30-kb fragment was determined to be 44 kb by length measurements as compared with 70 kb by intensity, and the 55-kb fragment was sized at 49 kb by length as compared with 88 kb by intensity. Given the limited sample number inherent in optical mapping, cross-checking the results with two sizing methods is extremely valuable.

Figure 2G illustrates three types of ordered restriction map produced by optical mapping as compared with published restriction maps (*10*). Additionally, Fig. 2, A to F, shows selected corresponding processed fluorescence micrographs of different yeast chromosomal DNA molecules digest-

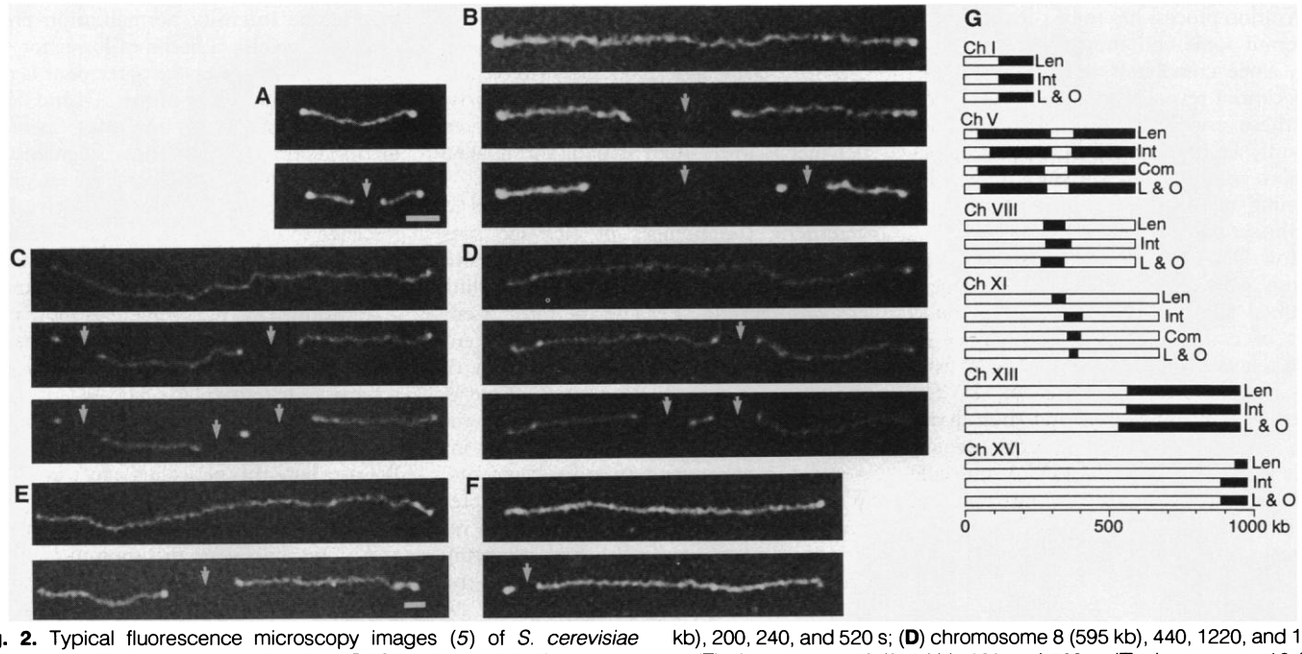

Fig. 2. Typical fluorescence microscopy images (*5*) of *S. cerevisiae* chromosomal DNA molecules stained with DAPI and embedded in agarose gel during Not I restriction endonuclease cleavage and corresponding restriction maps. Chromosomal DNA molecules were prepared and fixed as described (*4*). Images were background-corrected with the use of a smoothed and attenuated background image, smoothed, and stretched with 16-bit precision. Processing increases clarity but distorts intensity differences and some dimensionality. Images show evolution of Not I restriction digestion, with arrows highlighting cut sites. Intervals are timed after addition of Mg^{2+}. (**A**) Chromosome 1 (240 kb), 20 and 60 s; (**B**) chromosome 11 (675 kb), 500, 880, and 1160 s; (**C**) chromosome 5 (595 kb), 200, 240, and 520 s; (**D**) chromosome 8 (595 kb), 440, 1220, and 1360 s; (**E**) chromosome 13 (950 kb), 100 and 560 s; (**F**) chromosome 16 (975 kb), 460 and 560 s. Bars, 5 μm. A ×100 objective was used to image results in panels (A) through (D), and a ×63 objective was used for panels (E) and (F). A video tape showing these digests is available on request from the authors. (**G**) Graphical comparison of optical mapping results for Not I endonuclease restriction maps from *S. cerevisiae* chromosomal DNA molecules with published restriction maps (L & O) (*10*). Maps were constructed from length (Len), intensity (Int), or a combination of both (Com). Bar lengths for the optical mapping data are proportional to the means plotted in Fig. 1, and typical images are shown in Fig. 2.

ed with Not I (*4*). These images clearly show progressive digestion by the appearance of growing gaps in the fixed molecules. From such data, the order of fragments was determined by inspection of time-lapse images obtained every 20 s (*5*). Because observed molecules tend to move and can sometimes be confused with other molecules, inspection of a "cutting sequence" or "cutting movie" simplifies deconvolution of molecule-molecule interactions. Agreement was excellent between the optical- (length or intensity) and the electrophoresis-based maps. The third type of restriction maps (Com, Fig. 2G) combines length- and intensity-derived data: small restriction fragments (<60 kb) were sized by length, whereas intensity measurements provide the remaining fragment sizes needed to complete the maps.

Figure 2A shows images of a relatively small yeast chromosome (240 kb) that was elongated and fixed to roughly one-third of its contour length. Because chromosomal DNA molecules less than 350 kb relax quickly in molten agarose, they were trapped in an extended form at lower temperatures to hasten gelation. Note that molecular relaxation processes produced a gap and formed balls at the cut fragment ends, whereas the parental molecule ends remained essentially fixed. Molecules in this size range can form disproportionately large balls at parental molecule ends. Fragment relaxation motions at cut sites were generally observed to retrace the original gel pores occupied by uncut molecules, as predicted by polymer reptational theory (Figs. 2, A to F, and 3). These molecular characteristics were conserved regardless of molecular size and the number of cut sites. Fragments, approximately less than 90 kb, frequently relax completely to form balls as

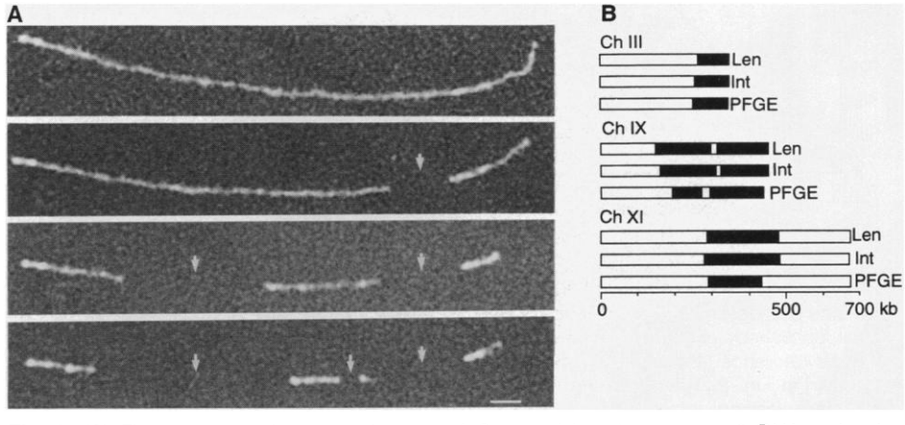

Fig. 3. (**A**) Fluorescence microscopy images of *S. cerevisiae* chromosome 9 DNA molecules stained with DAPI and embedded in agarose gel during Csp I restriction endonuclease cleavage and corresponding restriction maps. Chromosomal DNA molecules were digested and analyzed as in Fig. 2. Images show evolution of restriction digestion, with arrows highlighting cut sites, at 180, 360, 480, and 720 s. Bar, 5 μm. (**B**) Optical mapping results from Rsr II and Csp I endonuclease restriction digest of *S. cerevisiae* chromosomes 3, 9, and 11. Maps were constructed from fully cut length (Len) and intensity (Int) data and from pulsed-field gel electrophoresis (PFGE). Bar lengths are proportional to the calculated means (*12*). Rsr II and Csp I are isoschizomers.

shown in Figs. 2, B, C, and F, and 3. Restriction digestion results that vary in fragment number, size, and order can be used to readily characterize a mixture of similarly sized but different molecules. Figure 2, C and D, and Fig. 2, E and F, show results obtained from two such chromosomal mixtures. In the first example, a small distal restriction fragment on chromosome 5 (Fig. 2C) serves to differentiate it from chromosome 8. The second example (Fig. 2, E and F) shows that a single cut can differentiate similarly sized molecules, given sufficient resolution. These shear-sensitive, megabase-sized DNA molecules were mounted with minor breakage and mapped by means of a lower power (×63 as compared with ×100) microscope objective.

Figure 3 shows an ordered restriction map (and corresponding fluorescence micrographs) created from a Csp I digestion of chromosome 9 by optical mapping as compared to maps created by pulsed-field gel electrophoresis (PFGE) and hybridization with a series of genetically mapped sequences. Chromosomes 3 and 11 are as described (*12*). To avoid possible prejudicial selection and processing of image data, we first made the optical maps and then checked them with electrophoretically derived data. The overall agreement between the optical and pulsed electrophoresis maps is excellent, with the exception of the chromosome 9, 82-kb Csp I restriction fragment. This discrepancy may stem from mounting conditions, since chromosome 9 (Fig. 3A) was highly elongated (50%). Such molecules appear tautly stretched and exhibit less pooling of coil segments along their length. Although this degree of elongation can reduce image contrast, detection of small restriction fragments was enhanced so that a small 20-kb-sized fragment was clearly delineated (Fig. 3A, panel 4).

Large-scale maps are rarely made without error. Maps created by optical mapping may contain errors that stem from incorrect fragment number determination or the stated limits on precision of our fragment-sizing methods. DNAs that have nearly symmetric maps cannot be optimally averaged to improve resolution unless one end is identified, so that map polarity must be established through ancillary means. Given our levels of sizing precision, we believe that we probably do not consistently detect fragments below 30 kb, similar to the level of map resolution achieved by Link and Olson (*10*).

Optical mapping could be extended to mammalian genomes by technical advances that permit the detection and quantitation of restriction fragments (500 to 10,000 bp) generated by frequent-cutting enzymes. Ordered contigs of well-characterized fragments could then be constructed from high-resolution, ordered restriction maps created from randomly sheared genomic DNA, perhaps 500 kb in size. YACs or cosmids could also be similarly analyzed and compared with the genomic map, to facilitate ordering. Engineering advances in chamber design, sample handling, image analysis, and informatics should make a high throughput methodology available that is capable of rapidly mapping entire genomes and, more importantly, extending knowledge of sequence information to populations of individuals rather than to a prototype of each organism (*13*).

REFERENCES AND NOTES

1. I. Chumakov *et al.*, *Nature* **359**, 380 (1992); E. Maier *et al.*, *Nat. Genet.* **1**, 273 (1992).
2. D. T. Burke, G. F. Carle, M. V. Olson, *Science* **236**, 806 (1987).
3. L. Manuelidis, P. R. Langer-Safer, D. C. Ward, *J. Cell Biol.* **95**, 619 (1982); J. B. Lawrence, C. A. Villnave, R. H. Singer, *Cell* **52**, 51 (1988); H. H. Q. Heng, J. Squire, L. Tsui, *Proc. Natl. Acad. Sci. U.S.A.* **89**, 9509 (1992); G. van den Engh, R. Sachs, B. J. Trask, *Science* **257**, 1410 (1992).
4. Yeast chromosomal DNA (yeast strain AB972) was resolved by pulsed-field electrophoresis [D. C. Schwartz and C. R. Cantor, *Cell* **37**, 67 (1984)] using 1.00% Seakem low-melting agarose (FMC), 1/2× tris-borate EDTA (TBE; 42.5 mM Trizma base, 44.5 mM boric acid, 1.25 mM disodium EDTA). Cut gel bands were repeatedly equilibrated in TE [10 mM tris-HCl, 1 mM EDTA (pH 8.0)]. The gel-embedded, purified chromosomes were then equilibrated overnight at 4°C in Mg^{2+}-free restriction buffer containing acetylated bovine serum albumin (0.1 mg/ml), 1% β-mercaptoethanol, 0.1% Triton X-100 (Boehringer Mannheim, membrane quality), and 4,6-diamino-2 phenylindole dihydrochloride (DAPI; 0.2 μg/ml) with slow shaking. Equilibrated samples ranging in volume from 50 to 100 μl were melted at 72°C for 5 min and then cooled to 37°C. Approximately 0.3 to 0.5 μl of enzyme (2 to 14 U/μl) was spread on a slide. Enzyme reaction temperatures were as recommended by manufacturers. β-mercaptoethanol was added to discourage photolysis [M. Yanagida *et al.*, in *Applications of Fluorescence in the Biomedical Sciences*, D. L. Taylor *et al.*, Eds. (Liss, New York, 1986), pp. 321–345] and was tested at this concentration by electrophoresis for any deleterious effects on digestion. The melted sample (7 μl) was typically pipetted (slowly) by means of a wide bore pipette tip onto an 18 by 18 mm cover glass and rapidly deposited onto a slide. Timing and quenching of the gel is critical for control of elongation. The reaction chamber was then sealed with mineral oil to avoid evaporation, and the agarose was allowed to gel for at least 30 min at 4°C before diffusion of 50 mM $MgCl_2$ through an open space. For chromosomes 1 (240 kb) and 3 (345 kb), slides were in a cold desiccator (4°) before casting to hasten gelling, avoiding premature molecular relaxation. For the larger chromosomes, which relax more slowly, slides were kept at room temperature. The slide was placed on a temperature-controlled microscope stage at 37°C (except Csp I, 30°C). A high numerical aperture microscope objective can produce bright, high-contrast images of stained DNA molecules, but with a very shallow depth of focus. Experimentally, for a long molecule to be in focus, it must lie within a plane approximately 0.2 μm thick. Our method of gel fixation reproducibly allows visualization of molecules that are within this 0.2-μm tolerance as measured optically. We speculate that this degree of optical flatness results from a laminar, parabolic fluid flow pattern generated between the glass surfaces before gelation. Furthermore, dissolved agarose and DNA molecules may potentiate this effect by facilitating laminar flow, while preventing onset of turbulence.
5. DNA molecules were imaged using a Zeiss Axioplan or Axiovert 135 microscope equipped for epifluorescence (487901 filter pack for ultraviolet excitation and blue emission) and a ×100 or ×63 Plan-Neofluar objective (Zeiss) coupled to Hamamatsu C2400 SIT cameras. Care was taken to adjust the camera controls to avoid saturating the digitizer at either end of the intensity range. Every 20 s, 32 video frames were digitized to 8 bits and integrated to give 13-bit precision by a Macintosh-based Biovision image processor or a Pixelpipeline digitizer (Perceptics Corp.). A computer-controlled shutter was used to limit illumination to 1.5 s per image, giving a total of about 135 to 255 s for typical experiments. Neutral density filters were used to keep the illumination intensity measured at the objective below 100 μW. Control experiments showed no damage to DNA molecules under these conditions. Digitized images were recorded directly to disk and archived on tape.
6. Length and relative fluorescence intensity were calculated to 16-bit precision by means of a modified version of NIH Image for Macintosh by Wayne Rasband, available on request from the authors. Further details are available (manuscript in preparation). Briefly, the original unprocessed image was displayed in an enlarged format, and an overlay image was prepared by manual tracing of the DNA. The length map was made directly from this overlay. For intensity calculations, the 13-bit raw data image was smoothed and the overlay image was dilated five times to cover all foreground pixels. For each pixel marked on the overlay, a synthetic background value was calculated as the weighted average of surrounding pixels, with a weight that decreased with distance, but was zero for all marked pixels. These values are intended to approximate those which would have been measured had the DNA been absent. The intensity of a particular DNA fragment was the sum of all pixels of the fragment minus the matching background pixels. The area of the fragment was the original overlay dilated twice. This process was repeated for each frame of raw data that had an overlay image, excluding those with poor focus. Intensity results were averaged for five images after a cut, and the relative sizes of the two fragments were calculated as $x/(x + y)$ and $y/(x + y)$. If fragment y later cuts into u and v, then $[y/(x + y)][u/(u + v)]$ is used for the size of u. The resulting numbers constitute a single sample for the purposes of subsequent analysis.
7. The samples were averaged, and the 90% confidence interval on the mean was calculated by means of the t distribution with $n - 1$ df and the sample SD. This calculation is valid if the data represent random samples from a normal distribution. There is a 90% chance that the population mean falls within the confidence interval. For chromosome I, the reported confidence interval was found by taking the lower bound from the short fragments and the upper bound from the long fragments. The 90% confidence interval for the population SD (Fig. 1, inset graphs) was calculated with the sample SD, the number of samples, and the χ-square distribution with $n - 1$ df. The midpoint of this interval was used to estimate the population SD. The coefficient of variation (CV) is the estimated population SD divided by the sample mean. The pooled SD is the square root of the average of the variances. The relative error is the difference between our value and the reported value, divided by the reported value.
8. T. M. Roberts, G. D. Lauer, L. C. Klotz, *CRC Crit. Rev. Biochem.* **3**, 349 (1975); P.-G. de Gennes, *Scaling Concepts in Polymer Physics* (Cornell Univ. Press, Ithaca, 1979); D. C. Schwartz, thesis, Columbia University (1985); M. Doi and S. F. Edwards, *The Theory of Polymer Dynamics* (Oxford Univ. Press, New York, 1986); G. Holzwarth,

C. B. McKee, S. Steiger, G. Crater, *Nucleic Acids Res.* **15**, 10031 (1987); J. Noolandi, G. W. Slater, H. A. Lim, J. L. Viovy, *Science* **243**, 1456 (1989); J. Stellwagen and N. C. Stellwagen, *Nucleic Acids Res.* **17**, 1537 (1989); D. C. Schwartz and M. Koval, *Nature* **338**, 520 (1989); S. B. Smith, P. K. Aldridge, J. B. Callis, *Science* **243**, 203 (1989); S. Gurrieri, E. Rizzarelli, D. Beach, C. Bustamante, *Biochemistry* **29**, 3401 (1990); B. H. Zimm, *J. Chem. Phys.* **94**, 2187 (1991); E. D. T. Atkins and M. A. Taylor, *Biopolymers* **32**, 911 (1992).

9. We scored cutting frequencies by counting cuts in molecules present in microscope fields (containing typically three to five molecules). About half of the fields showed no cutting and were not scored, resulting in an underestimate of the number of uncut molecules. The cutting frequency results for chromosome 5 digested with Not I show that the number of fully cut molecules is approximately half that of all singly cut molecules: we calculate the value corresponding to complete digestion by assuming that an equal distribution of identically sized chromosome 5 and 8 DNA molecules are present in the mounted sample. The Not I restriction maps for these chromosomes reveal that chromosome 5 has three cut sites, whereas chromosome 8 has only two. Chromosome 11 cutting frequency data are different: 25% of all cut molecules are seen to be fully digested (two cutting sites). An explanation for the apparently lower frequency is that this chromosome produces a 30-kb-sized Not I fragment that is more difficult to detect optically than larger fragments. Observation of 1000-kb-sized molecules such as chromosome 13 and 16 shows that roughly half of the molecules are digested to completion (one cut) in mounts with scorable cutting activity.
10. A. J. Link and M. V. Olson, *Genetics* **127**, 681 (1991).
11. Absolute intensities from individual images (Not I fragments from chromosomes 1 and 11) were calculated (*6*) and plotted against change of apparent length over a time interval typically used in optical mapping (10 to 15 min). Data from images with poor focus were discarded. For each sample, we calculated the initial intensity by averaging absolute intensity values from groups of five adjacent images and taking the largest value. We normalized the values from several samples by dividing values from each image by the initial intensity for the sample.
12. A collection of genetically mapped Southern (DNA) hybridization probes were used to create ordered PFGE restriction maps for comparison with optical mapping results: Chromosome 3 (*LEU2, MAT*), chromosome 9 (*THS1, SEC11, SUC2, CAP2*), chromosome 11 (*SIR1, MAK11, URA1, APE2*). Relative apparent length results are given assuming random sampling from a normal population. When the number of samples is less than six, the pooled SD from the Not I results is used to calculate the confidence interval. Chromosome enzyme (our PFGE size/total size), mean ± 90% confidence kb/population SD ± 90% confidence kb (number of samples): 3 Rsr II (250/350) 264 ± 31/58 ± 25 (8), 3 Rsr II (95/350) 86 ± 31/58 ± 25 (8); 11 Csp I (292/675) 288 ± 30/72 ± 23 (14), 11 Csp I (143/675) 193 ± 43/101 ± 32 (14), 11 Csp I (240/675) 194 ± 27/65 ± 21 (14); 9 Csp I (145.5/455) 138 ± 35/47 (5), 9 Csp I (20/455) 17 ± 35/47 (5), 9 Csp I (82/455) 151 ± 35/47 (5), 9 Csp I (194/455) 149 ± 35/47 (5). Relative fluorescence intensity results after two dilations of backbone, assuming random sampling from a normal population. Chromosome enzyme (our PFGE size/total size), mean ± 90% confidence kb/population SD ± 90% confidence kb (number of samples): 3 Rsr II (250/350) 256 ± 20/37 ± 16 (8), 3 Rsr II (95/350) 94 ± 20/37 ± 16 (8); 11 Csp I (292/675) 279 ± 24/45 ± 20 (8), 11 Csp I (143/675) 204 ± 33/61 ± 27 (8), 11 Csp I (240/675) 191 ± 20/38 ± 17 (8); 9 Csp I (145.5/455) 128 ± 34/36 (3), 9 Csp I (20/455) 14 ± 34/36 (3), 9 Csp I (82/455) 150 ± 34/36 (3), 9 Csp I (194/455) 163 ± 34/36 (3).
13. L. L. Cavalli-Sforza, *Am. J. Hum. Genet.* **46**, 649 (1990).
14. We thank I. Maity and M. Hsu for technical assistance, N. Kallenbach for helpful suggestions, and N. Seeman and his laboratory for synthesis of oligonucleotides. Supported by grants from the NIH (HG00225-01), the NSF, the W. M. Keck Foundation, and the Lucille P. Markey Charitable Trust. D.C.S. is a Lucille P. Markey Scholar.

19 February 1993; accepted 10 June 1993

Erythrocyte P Antigen: Cellular Receptor for B19 Parvovirus

Kevin E. Brown,* Stacie M. Anderson, Neal S. Young

The pathogenic human parvovirus B19 replicates only in erythroid progenitor cells. This virus was shown to bind to blood-group P antigen, as measured by hemagglutination. Erythrocytes lacking P antigen were not agglutinated with B19. Purified P antigen (globoside) blocked the binding of the virus to erythroid cells and the infectivity of the virus in a hematopoietic colony assay. Target cells were protected from infection by preincubation with monoclonal antibody to globoside. Knowledge of a parvovirus receptor has implications for understanding the pathogenesis of parvovirus infections and for the use of parvoviruses in gene therapy.

The only known pathogenic human parvovirus, B19 parvovirus, causes the common illness fifth disease in normal individuals (*1*), transient aplastic crisis in patients with underlying hemolysis (*2*), and chronic anemia from persistent infection in immunocompromised patients (*3*). Parvovirus infection in pregnancy can lead to hydrops fetalis and fetal loss (*4*) or congenital infection (*5*). In contrast to most viruses, B19 parvovirus is tropic for one highly differentiated cell type, the human erythroid progenitor, and tropism might be mediated by a cellular receptor unique to cells of the erythroid lineage. Cellular receptors are known for influenza A, rabies, human immunodeficiency and Epstein-Barr viruses, as well as several of the picornaviruses (*6*), but none has been described for any of the *Parvoviridae*.

Most parvoviruses can agglutinate erythrocytes, and the results of early attempts to remove the hemagglutinin of rodent parvoviruses from guinea pig erythrocytes by chemical methods or neuraminidase suggested that binding might be mediated by a glycolipid (*7*). Enzymatic treatment of target cells in binding assays implicated sialic acid in the context of a glycoprotein for the hemagglutination of feline panleukopenia virus (*8*) and the cellular binding of minute virus of mice, a rodent parvovirus (*9*). These results all suggest the importance of carbohydrate antigens for parvovirus binding. However, the precise nature of the receptor is not known for any of these viruses.

We have shown that B19 parvovirus empty capsids (*10*) agglutinated human red cells (*11*), and we tested the ability of membrane extracts from different cell types to block B19 binding. Membrane extracts were prepared by means of 10 mM CHAPS to solubilize proteins and lipids. Extracts from human erythrocyte ghosts (*12*) or cells permissive for B19 parvovirus [human bone marrow and UT-7 leukemic cells (*13*)] blocked hemagglutination. In contrast, extracts from K562, HL-60, and HeLa cells, which are not permissive for the virus, did not block binding.

Trypsin (0.2%; 1 hour at 37°C) and neuraminidase (0.1 U ml^{-1}; 1 hour at 37°C) each increased binding (a 4 log_2 and a 3 log_2 increase in hemagglutination (HA) titer, respectively), suggesting that protein and sialic acid were not involved and that modification of the red cell membrane by these agents might expose binding sites. Treatment with sodium periodate (10 mM; 15 min at 37°C) markedly reduced the binding of virus to erythrocytes [>4 log_2 decrease in HA titer (5 μM sodium periodate treatment overnight did not reduce binding)], implicating carbohydrates other than sialic acid. Phosphoinositol-specific phospholipase C and reducing agents did not affect binding.

Human erythrocyte ghosts (*12*) were then treated with CHAPS, the solubilized extract was incubated with agarose-immobilized enzymes overnight at 37°C, and the supernatant was tested in the hemagglutination inhibition assay (*11*). Pretreatment of red cell extract with immobilized phospholipase A_2 removed activity completely, whereas treatment with immobilized proteases had no significant effect. These results suggest that the inhibitor was either a lipid or that a lipid was important in maintaining

Hematology Branch, National Heart, Lung and Blood Institute, Bethesda, MD 20892.

*To whom correspondence should be addressed.